Time-lapse Full Waveform Inversion: Synthetic and Real Data Examples

Espen Birger Raknes, Wiktor Weibull, and Børge Arntsen, Norwegian University of Science and Technology*

SUMMARY

Time-lapse seismic data contains information about changes in the subsurface, and are nowadays used as an effective tool to characterize changes in reservoirs due to production of oil and gas or injection of CO_2. The full waveform inversion (FWI) method can be used to detect these changes. Three different approaches for time-lapse FWI are presented: (1) performing independent inversion for each dataset, and then compare the inversion results; (2) first invert for one of the datasets and then use the end model from the first inversion as initial model for the inversion for the other datasets; (3) similar to (2), but the data consists of a combination of the optimal data of previous inversion and the difference between the observed datasets. The three approaches are applied on synthetic and real time-lapse marine streamer seismic data. The approaches are able to detect and describe the changes in velocities in the subsurface.

INTRODUCTION

Time-lapse seismic data contains information about changes in the subsurface and is used as a dynamic tool for monitoring a reservoir during its production lifetime and for monitoring injection of CO_2. Time-lapse data has proven to be an effective tool in reservoir imaging (Biondi et al., 1996; Johnston et al., 1998), and for monitoring of CO_2 injected in the subsurface (Lumley et al., 2003; Lumley, 2010).

The full waveform inversion (FWI) method is a technique for estimating parameters affecting wave propagation using inverse theory (Virieux and Operto, 2009). The method has been successfully applied to estimate wave velocities using real field data (Liu et al., 2012). Using the FWI method in combination with time-lapse data it is possible to quantify changes in reservoirs (Zheng et al., 2011; Routh et al., 2012).

There exist different approaches for applying FWI on time-lapse data. The naive approach is based on doing independent inversions of the different datasets in the time-lapse data, and then calculate the difference between the obtained models from the inversions. Another approach is formed by first inverting for the first dataset, and the resulting model is then used as input in the inversion for the next dataset. Recently, a relatively similar approach where, in addition, the observed dataset is slightly modified by adding the observed data residuals to the synthetic data from the first inversion, was developed (Zheng et al., 2011). The three approaches have been applied on synthetic data with success.

In this study, we try the above mentioned approaches on both synthetic and real time-lapse data where we estimate velocity changes in the subsurface. The synthetic example is a realistic model of the Gullfaks field, where we simulate time-lapse changes by varying the fluid content in the reservoir. For the real data example we use datasets from a field in the Norwegian North sea, where gas leaked from one of the producing wells into subsurface formations. The first dataset was acquired before the leakage and the second dataset was acquired after the leakage. Thus, there exist differences in the two datasets which the FWI method should be able to quantify.

TIME-LAPSE FULL WAVEFORM INVERSION

The FWI method is an algorithm which (iteratively) searches for a model that describes given data, by gradually minimizing a given objective function. In seismic inversion problems, the objective function is a measure of the dissimilarity between measured data, and data modeled using the current inverted model; when the two models are similar, the datasets should also be similar. In general terms the inverse problem is simply written as:

$$\text{Find } \mathbf{m} \text{ such that } S(\mathbf{m}) \text{ is minimized.} \tag{1}$$

Here, $\mathbf{m}$ is the model and $S(\mathbf{m})$ is the objective function. Searching for the minimum is done using an iterative minimization algorithm (Nocedal and Wright, 2006), which in general terms is written as

$$\mathbf{m}_{k+1} = \mathbf{m}_k - \alpha_k \mathbf{g}_k, \tag{2}$$

where $\alpha_k > 0$ is the step length and $\mathbf{g}_k$ is the gradient of $S(\mathbf{m})$ with respect to $\mathbf{m}$, at step k. The algorithm requires an initial model, from which it iterates until some convergence criteria are fulfilled. The model from the last iteration is then the model describing the observed data best.

Using the adjoint state method (Tarantola, 1984), the gradient at iteration k can be calculated as a zero-lag cross-correlation between two wave fields,

$$\mathbf{g}_k = \sum_{shots} \int_0^T \overrightarrow{\psi}(\mathbf{m}_k, t) \overleftarrow{\psi}(\mathbf{m}_k, t)\, dt, \tag{3}$$

where $\overrightarrow{\psi}(\mathbf{m}_k, t)$ is a wave field forward propagated from the source position, and $\overleftarrow{\psi}(\mathbf{m}_k, t)$ is a backward propagated wave field where the data residuals are used as sources at the receiver positions. For more details and examples about the FWI method, see Virieux and Operto (2009) and the references given therein.

One of the major issues with the FWI method is the local/global minima challenge. The ideal solution to eq. (1) using an iterative method is the global minimum. In practice, finding the global minimum of the problem is difficult due to the strong non-linearity in the problem, many unknowns, and high computational requirements. The iterative optimization method in eq. (2) is a local search algorithm, which not always approach the global minimum. Thus, the algorithm may be trapped in a local minima basin. To avoid cycle skipping (Virieux and

DOI http://dx.doi.org/10.1190/segam2013-0540.1

Operto, 2009), and convergence towards an acceptable solution, a good starting model is necessary. One strategy to create reliable initial models is by using wave equation migration velocity analysis (WEMVA) (Weibull et al., 2012).

Time-lapse FWI can be formulated in several ways. In this study we use three different approaches. Assume that two different datasets are observed at different times T_i, and denote the dataset at T_1 for $\mathbf{d}_{base}$, and the dataset at T_2 for $\mathbf{d}_{mon}$. The dataset at T_1 is referred to as the base dataset, and the dataset at T_2 is referred to as the monitor dataset. In the *first approach* two independent inversions are performed using $\mathbf{d}_{base}$ and $\mathbf{d}_{mon}$. To reveal the changes in the models the two output models are compared. The *second approach* is formed by first running the inversion on $\mathbf{d}_{base}$. Then the resulting model is used as initial model for the inversion for $\mathbf{d}_{mon}$. At the end the two models are compared (Routh and Anno, 2008). In the *third approach* the inversion for $\mathbf{d}_{base}$ is done first and the resulting model is used as start model for the inversion for $\mathbf{d}_{mon}$. The observed data $\mathbf{d}_{base}$ is, in addition, modified as follows

$$\widehat{\mathbf{d}}_{base} = \mathbf{d}_n + (\mathbf{d}_{mon} - \mathbf{d}_{base}) = \mathbf{d}_n + \Delta\mathbf{d}, \qquad (4)$$

where $\mathbf{d}_n$ is the synthetic data from the last step of the inversion for $\mathbf{d}_{base}$ (Zheng et al., 2011).

There are some differences between the three approaches that are worth mentioning. The two inversions in the first approach are performed independently. Thus, the convergence of the two inversions must be consistent with each other, otherwise the inversions may introduce artifacts in the time-lapse images. The initial model for the base inversion in the two other approaches is relatively close to the ending model for the monitor inversion. Therefore, the convergence of the monitor inversion is faster compared to the base inversion. One can say that the data residuals acts as "forces" in the monitor inversion in the second and third approaches, which give strong constraints on the monitor inversion. Therefore, the amount of possible inversion artifacts is also reduced. The modification of the dataset in the third approach reduces the possible inversion artifacts even further.

RESULTS

We test the three approaches using both synthetic and real data. The synthetic example is created using a model of the Gullfaks field. Time-lapse field data from the Norwegian North Sea is used in the real example.

Synthetic Example

The synthetic data is created with the use of a model of the Gullfaks field, see Figure 1. The interesting part in the model is the reservoir at the crest of the rotated fault blocks (approximately position 5000 m and 1950 m depth). To create time-lapse data we use two versions of the model; we define the base case when the reservoir is filled with oil, and the monitor case when the reservoir is filled with water. Between the two models there are P-wave velocity changes in the range $0-153$ m/s, and the changes are only locally within the reservoir.

Using the two models we simulate a marine streamer survey

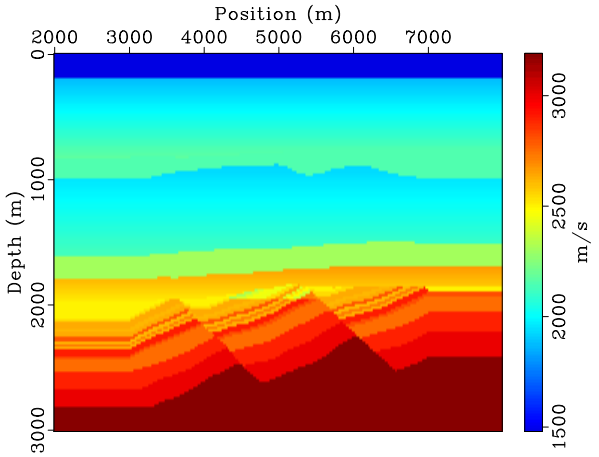

Figure 1: The true model for the P-wave velocity. The reservoir of interests is located at the top of the middle faults, at approximately 5000 m position and 2000 m depth.

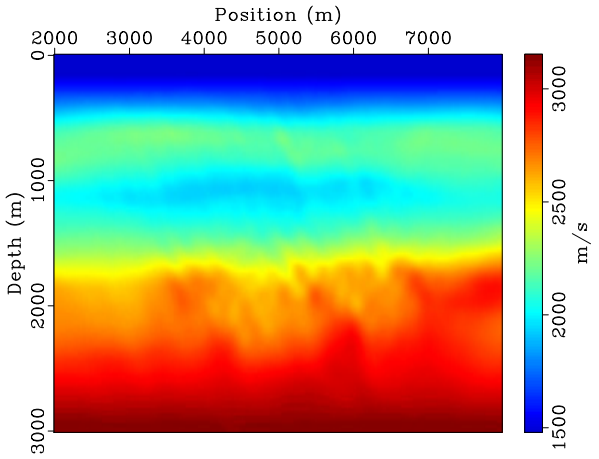

Figure 2: The initial model for the P-wave velocity.

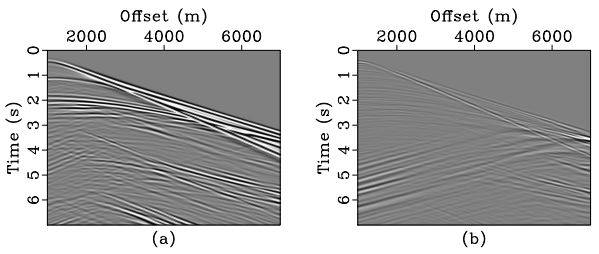

Figure 3: Data residual at the first (a) and last (b) iteration for the inversion using the base dataset. A time-gain has been applied.

DOI http://dx.doi.org/10.1190/segam2013-0540.1

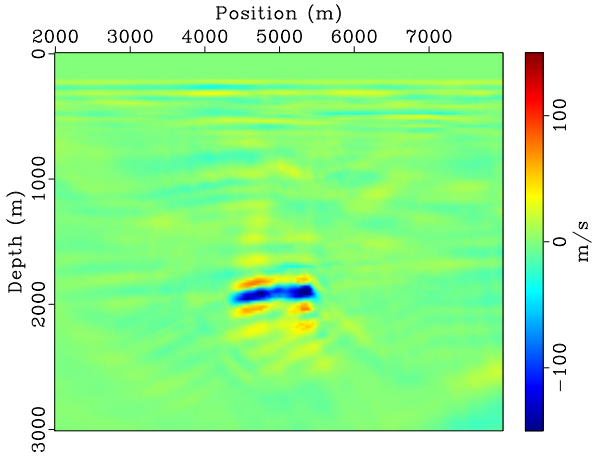

Figure 4: Synthetic example time-lapse image for approach one.

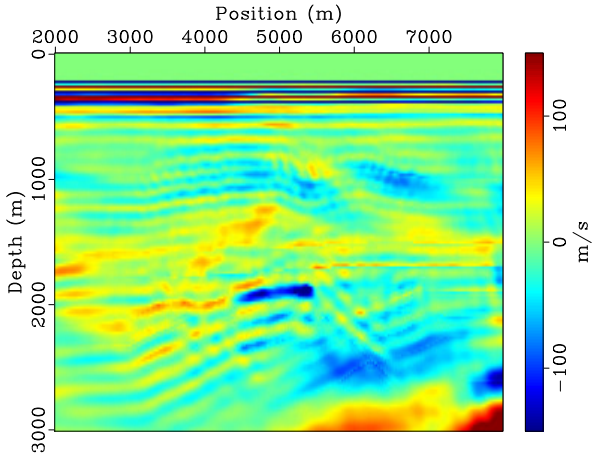

Figure 5: Synthetic example time-lapse image for approach two.

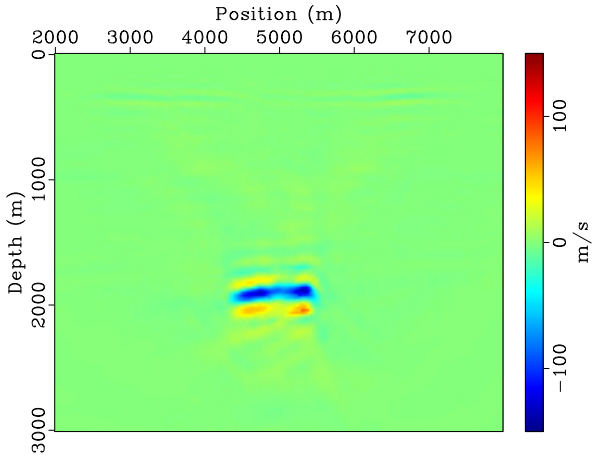

Figure 6: Synthetic example time-lapse image for approach three.

consisting of 370 shots with a 6 km streamer. The streamer has 300 receivers which are separated by 20 m. The shot interval is 20 m. The source wavelet is a Ricker wavelet with a peak frequency of 5.0 Hz. The WEMVA method is used to produce the initial model for the inversions, see Figure 2.

A comparison of a shot residual at the first and last inversion step is shown in Figure 3. The figure shows a good match between the observed and simulated datasets, and thus the inversion is able to find a model which describe the data. The time-lapse FWI results using approach one is given in Figure 4, approach two in Figure 5, and approach three in Figure 6. All three approaches are able to give the correct velocity change in the reservoir. Some artifacts right above and below the reservoir are visible, and approach three seems to have the smallest artifacts. Approach two suffers from large differences between the two inversions all over the model.

Real Example

The time-lapse real dataset is recorded over a field in the Norwegian North Sea. The base dataset was acquired in 1988 and the monitor dataset was acquired in 1990. Between the two surveys the field was exposed to a leakage in one of the producing wells. Each of the two datasets consists of 230 shots. The streamer has 95 receivers with a spacing of 12.5 m, and the total length is 1253 m. The datasets are regularized into the same geometry, scaled and filtered with a bandpass filter with the band $0-15$ Hz, before they are used in the inversions. Similar to the synthetic example the initial model for the inversion is produced using the WEMVA method.

The time-lapse FWI results for approach one are given in Figure 7. The blow-out well is placed at position 3400 m in the figure. From other types of analysis of the datasets, an anomaly at $450-500$ m below the well is a well-known time-lapse effect. This anomaly is a result of gas leaking into the formations, which resulted in an decrease in the velocities of the rocks. From the image in Figure 7 a clear anomaly is visible at $450-500$ m depth. In addition, a chimney shaped effect is visible below the anomaly. Figure 8 shows the results of the inversion using the second approach. The anomaly is visible on the inversion results, though not as large as in the first approach. The chimney pattern is not visible in the image. The inversion results using approach three are provided in Figure 9, and the image is very similar to the image using approach two.

Working with real data involves uncertainties. One of the major uncertainties in time-lapse data is the repeatability of the data, which in practice is very difficult to achieve. Noise is also another type of uncertainty that affects the inversion. In all the results strong time-lapse effects are visible in the sea bottom (at 100 m depth), which in addition differs between the three images. These time-lapse effects are not present in the field, and thus are regarded as artifacts from the inversions. For approach two and three, repeated oscillations in depth are visible in the images. These artifacts may be explained by the narrow band frequency content of the real dataset.

To speed up the convergence and improve the inversion results, a common approach is to apply regularization in $S(\mathbf{m})$. In our

DOI http://dx.doi.org/10.1190/segam2013-0540.1

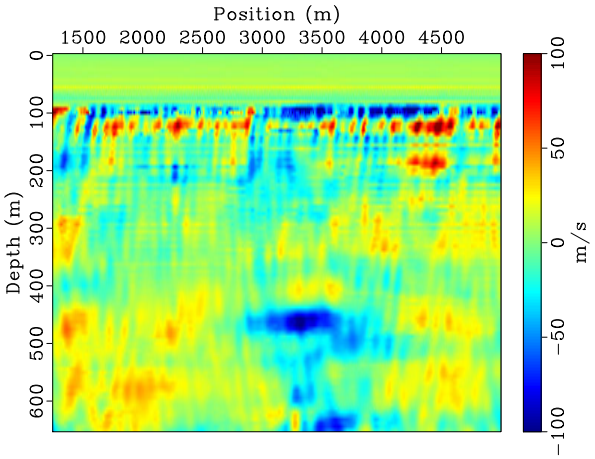

Figure 7: Real example time-lapse image for approach one.

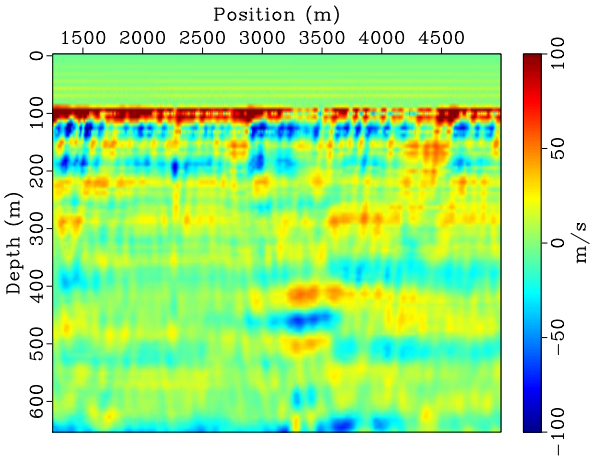

Figure 8: Real example time-lapse image for approach two.

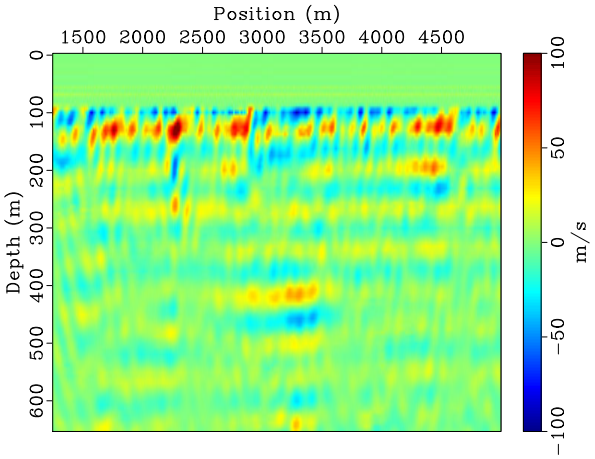

Figure 9: Real example time-lapse image for approach three.

inversions no regularization was applied, and this might, in addition to the above mentioned uncertainties, explain the instability of the results, especially for the real example.

CONCLUSION

In this study we have applied three different approaches for time-lapse FWI on synthetic and real time-lapse seismic data. All three approaches are able to recover time-lapse changes in the velocities. The differences in the time-lapse images between the three approaches are large. The third approach gave the best images for the synthetic example. Hence, an time-lapse FWI approach where one uses the base model in combination with some data modification, give strong constraints on the inversions. As a result, the approach is able to detect local time-lapse changes in the models, and the inversion converges relatively fast. The images for the three approaches using real time-lapse data are different, and include several uncertainties that may be explained by the lack of repeatability of the data, noise and narrow frequency band in the data. However, the approaches are able to detect a well-known gas leakage into a subsurface formation, though with differences in the size of the gas anomaly.

ACKNOWLEDGMENTS

We thank the BIGCCS centre, the ROSE Consortium and Statoil Petroleum AS for financing this research.

DOI http://dx.doi.org/10.1190/segam2013-0540.1

http://dx.doi.org/10.1190/segam2013-0540.1

EDITED REFERENCES

Note: This reference list is a copy-edited version of the reference list submitted by the author. Reference lists for the 2013 SEG Technical Program Expanded Abstracts have been copy edited so that references provided with the online metadata for each paper will achieve a high degree of linking to cited sources that appear on the Web.

REFERENCES

Biondi, B., C. Deutsch, R. Gundesø, D. Lumley, G. Mavko, T. Mukerji, J. Rickett, and M. Thiele, 1996, Reservoir monitoring: A multidisciplinary feasibility study: 66th Annual International Meeting, SEG, Expanded Abstracts, 1775–1778.

Johnston, D., R. McKenny, J. Verbeek, and J. Almond, 1998, Time-lapse seismic analysis of fulmar field: The Leading Edge, **17**, 1420–1428, http://dx.doi.org/10.1190/1.1437864.

Liu, F., L. Guasch, S. A. Morton, M. Warner, A. Umpleby, Z. Meng, S. Fairhead, and S. Checkles, 2012, 3D time-domain full waveform inversion of a Valhall OBC data set: 82nd Annual International Meeting, SEG, Expanded Abstracts, 1–5.

Lumley, D., 2010, 4d seismic monitoring of CO_2 sequestration: The Leading Edge, **29**, 150–155, http://dx.doi.org/10.1190/1.3304817.

Lumley, D., D. C. Adams, M. Meadows, S. Cole, and R. Wright, 2003, 4D seismic data processing issues and examples: 73rd Annual International Meeting, SEG, Expanded Abstracts, 1394–1397.

Nocedal, J., and S. J. Wright, 2006, Numerical optimization, 2nd ed.: Springer Science Business Media, LLC.

Routh, P., G. Palacharla, I. Chikichev, and S. Lazaratos, 2012, Full wavefield inversion of time-lapse data for improved imaging and reservoir characterization: 82nd Annual International Meeting, SEG, Expanded Abstracts, 1–6.

Routh, P. S., and P. D. Anno, 2008, Time-lapse noise characterization by inversion: 78th Annual International Meeting, SEG, Expanded Abstracts, 3143–3147.

Tarantola, A., 1984, Inversion of seismic reflection data in the acoustic approximation: Geophysics, **49**, 1259–1266, http://dx.doi.org/10.1190/1.1441754.

Virieux, J., and S. Operto, 2009, An overview of full-waveform inversion in exploration geophysics: Geophysics, 74, no. 6, WCC1–WCC26.

Weibull, W., B. Arntsen, and E. Nilsen, 2012, Initial velocity models for full waveform inversion: 82nd Annual International Meeting, SEG, Expanded Abstracts, 1–4.

Zheng, Y., P. Barton, and S. Singh, 2011, Strategies for elastic full-waveform inversion of time-lapse ocean bottom cable (OBC) seismic data: 81st Annual International Meeting, SEG, Expanded Abstracts, 4195–4200.